Available online at www.sciencedirect.com
ScienceDirect
International Journal of Heat and Mass Transfer 49 (2006) 4773–4785
International Journal of HEAT and MASS TRANSFER
www.elsevier.com/locate/ijhmt

2D natural convection flows in tilted cavities: Porous media and homogeneous fluids

Elsa Báez, Alfredo Nicolás *

Depto. Matemáticas, 3er Piso Ed. AT-Diego Bricio, UAM-I, 09340 México, DF, Mexico

Received 14 December 2005; received in revised form 3 June 2006
Available online 7 September 2006

Abstract

Natural convection flows are studied numerically for porous media and homogeneous fluids inside a rectangular cavity with inclination. These thermal fluid flows are considered under the respective two-dimensional unsteady Boussinesq approximation in stream function and vorticity variables. The study depends on the Rayleigh number, angle of inclination, and the aspect ratio of the cavity. At the validation stage our results are in good agreement with those reported by other authors. Results suppose to be new are presented either for angles of inclination not reported before or for high Rayleigh numbers with large aspect ratios. In rectangular porous cavities with Rayleigh number $\geqslant 10^2$ multiple cells appear for some angles. In homogeneous fluids, for Rayleigh numbers of the order of 10^5–10^6 in large enough vertical cavities at most secondary cells appear for some angles and the flow becomes more complex and looks like to be oscillatory.

1. Introduction

The mass and momentum equations in natural convection fluid flow are given by the Darcy equations in porous media and by the Navier–Stokes equations in homogeneous fluids, and both are coupled with the thermal energy equation through the unsteady Boussinesq approximation to deal with an incompressible structure in both situations. Besides, in this work the dimensionless problems are formulated in terms of the stream function and vorticity variables; then, the computation of the pressure is avoided and the incompressibility condition is satisfied automatically.

Our numerical study on natural convection flows is carried out on tilted rectangular cavities (tall, wide or square). Once a convenient second order time discretization is performed, non-linear elliptic systems are obtained; they are solved through a fixed point iterative process with a common structure for both problems. The iterative process leads to the solution of uncoupled, well-conditioned, symmetric linear elliptic problems for which very efficient solvers exist regardless of the space discretization.

The study on natural convection flows in porous media and homogeneous fluids has important technological applications. To name a few: storage and preservation of grains and cereals, solar energy collectors, filter systems, and transport of radioactive wastes through the soil, in the first case; energy storage systems, security on nuclear reactors, thermal insulation for buildings, cooling of electronic devices, and geophysical applications, in the second case. On the parameters, Rayleigh number, angle of inclination ϕ and aspect ratio A ($A =$ ratio of the height to the width) of the cavity that characterize the evolution of the flow, by its definition, we must distinguish between the Rayleigh number of a fluid in a porous medium Ra_{p} and the one of a homogeneous fluid Ra_{h}.

Some works are mentioned next in connection with natural convection problems in both fluids subjected to a temperature gradient on two opposite walls of the cavity and the other two being insulated, which is the subject to deal with in this work. (I) *Porous media*: Moya et al. [1] solve the steady problem in tilted horizontal rectangular cavities

* Corresponding author. Tel.: +52 55 5804 4656; fax: +52 55 5804 4660.
E-mail address: anc@xanum.uam.mx (A. Nicolás).

0017-9310/$ - see front matter © 2006 Elsevier Ltd. All rights reserved.
doi:10.1016/j.ijheatmasstransfer.2006.06.011

with Rayleigh numbers $Ra_p = 10^2$, finding multiple cellular flow. Sen et al. [2] from de steady problem also study the multiplicity of solutions considering vertical and horizontal inclined cavities, showing analytical and numerical results for small angles ϕ and $Ra_p \leqslant 500$. Baytas [3] shows results from the unsteady problem in a tilted square cavity for $Ra_p = 10^2, 10^3, 10^4$; Saeid and Pop [4] study the transient evolution for these Rayleigh numbers in a square cavity, reporting the final time when the steady state is reached. In connection with works more concerned with applications we can mention Bennacer et al. [5], Al-Amiri [6], Slimi et al. [7], Das and Morsi [8], Slimi et al. [9]. (II) *Homogeneous fluids*: Hamady et al. [10] study from the unsteady problem the effect of the inclination on the heat transfer inside an enclosure with square cross section for Ra_h in $10^4 < Ra_h \leqslant 10^6$. Henkes and Hoogendoorn [11] present results from the steady problem in a square cavity when Ra_h is increased in the range $10^3 \leqslant Ra_h \leqslant 10^8$. In Bermúdez and Nicolás [12] flows for Ra_h in $10^5 \leqslant Ra_h \leqslant 10^8$ inside a square cavity are reported from the unsteady problem in primitive variables. On the other hand, flow in a differentially heated tall cavity with aspect ratio 8 have been studied by some authors using an alternative dimensionless set of equations in the unsteady problem, mainly in primitive variables. Christon et al. [13] seem to be the first authors to establish the guide questions about the behavior of the fluid in this kind of cavities at high Rayleigh numbers Ra_h. In this direction, and for the specific value $Ra_h = 3.4 \times 10^5$, the following works can be mentioned: Xin and Le Quéré [14] investigate the bifurcation points and the stability of the solutions. Auteri and Parolini [15] investigate the first instabilities and report a phenomenon of symmetry breaking, which is restored later, providing the first steps on transition to chaos. In Glowinski [16], results are reported at different times, showing that the flow is time-dependent, that is, the flow does not reach a steady state.

The results in this work show that either the solution reaches the steady state of the flow, if it exists, or describes the evolution of a time-dependent flow when a steady state is not reached since the flow may be oscillatory. In porous media some results are validated in tilted rectangular cavities. Results, supposed to be new, are shown for $Ra_p \geqslant 10^2$. In homogeneous fluids, results are reported for $Ra_h = 3.4 \times 10^5$ in a tall cavity without inclination to validate the numerical method with time-dependent flows, taking into account that the validation in square cavities until $Ra_h = 10^5$, reaching a steady state, is given in Báez et al. [17]. Results, supposed to be also new, are shown in tilted square cavities for the higher $Ra_h = 10^6$ and in cavities with height $\leqslant 8$ for $Ra_h \leqslant 10^6$. All the results are complemented with their local and global Nusselt numbers on the hot wall, and the extreme values of the stream function. The turbulence phenomenon, which some authors claim occurs for $Ra_h \geqslant 10^6$, is not addressed here since to our knowledge it depends on the kind of non-dimensional equations used, then even though two non-dimensional situations are considered in our numerical experiments they are not pointing in this direction yet.

Summing up, some results are presented as a validation matter, mainly flows reached at steady state from the unsteady problem agreeing with the ones other authors have obtained from the steady problem; others are new, either extended to a higher Rayleigh number or considering angles of inclination no reported so far as well as results with different aspect ratios. To assure that the new flows are correct, to our knowledged reported for the first time, a time step and mesh independence studies are made. Finally, some similarities and differences between porous media and homogeneous fluids are described.

2. Mathematical models

Natural convection flow of a thermal viscous fluid assumed to be Newtonian is considered under the Boussinesq approximation in the presence of a gravitational field. The Boussinesq approximation is based on the assumptions that the temperature variations are small enough in order to consider the density ρ as a constant except in the buoyancy term $\rho\mathbf{g}$, where $\mathbf{g}$ is the gravitational force and ρ, from the state equation, is given linearly by $\rho = \rho_0[1 - \beta(T - T_0)]$ where T is the temperature, the density change due to changes in pressure is neglected, and ρ_0 and T_0 denote reference density and temperature respectively; fluid properties, such as dynamic viscosity μ, the permeability K, thermal expansion $\beta = -\frac{1}{\rho_0}(\frac{\partial\rho}{\partial T})_p$, the thermal diffusivity η, and the specific heat c_p are assumed to be constants; and the dissipation of mechanical energy is neglected, Gunzburger [18], Landau and Lifshitz [19], Leal [20]. The first of these assumptions leads us to consider these thermal fluids under an incompressible structure.

Let $\Omega \subset \mathbb{R}^N$ $(N = 2, 3)$ be the region of the flow of an unsteady, viscous, and thermal fluid; and Γ its boundary. Under the Boussinesq approximation this kind of flows may be governed by the following dimensionless vector systems, in Ω and $t > 0$

(pm):

$$\mathbf{u} + \nabla p = Ra_p\theta\mathbf{e} \tag{1}$$

$$\nabla \cdot \mathbf{u} = 0 \tag{2}$$

$$\theta_t - \nabla^2\theta + \mathbf{u} \cdot \nabla\theta = 0, \tag{3}$$

(hf):

$$\mathbf{u}_t - \nabla^2\mathbf{u} + \nabla p + (\mathbf{u} \cdot \nabla)\mathbf{u} = \frac{Ra_h}{PrRe^2}\theta\mathbf{e} \tag{4}$$

$$\nabla \cdot \mathbf{u} = 0 \tag{5}$$

$$\theta_t - \frac{1}{PrRe}\nabla^2\theta + \mathbf{u} \cdot \nabla\theta = 0 \tag{6}$$

where (pm) denotes porous media and (hf) homogeneous fluids; $\mathbf{u}$ and p are the dimensionless primitive variables velocity and pressure, and θ the temperature. In porous media: $\mathbf{u} = \frac{\mathbf{v}L_0}{\eta}$, $p = \frac{K}{\mu\eta}(P - \rho_0 g y)$, and $\theta = \frac{T - T_0}{T_h - T_c}$, in homoge-

neous fluid: $\mathbf{u}=\frac{\mathbf{v}}{U_0}$, $p=\frac{P-\rho_0 g y}{\rho_0 U_0^2}$, and $\theta=\frac{T-T_0}{T_h-T_c}$; where L_0, T_0, T_h, T_c, ρ_0, and U_0 are reference quantities of longitude, temperature, density, and velocity. Eqs. (1) and (2) are the Darcy equations whereas (4) and (5) the Navier–Stokes equations, coupled with the temperature Eqs. (3) and (6) respectively; (2) and (5) are known as the *incompressibility condition*, and **e** is the unitary vector in the direction of **g**. The parameter Ra_p is the Rayleigh number of the porous medium; Ra_h, Re, and Pr are the Rayleigh, Reynolds, and Prandtl numbers of the homogeneous fluid. These parameters are given by $Ra_p=\frac{K\beta L_0 g(T_h-T_c)}{\eta\nu}$, $Ra_h=\frac{\beta L_0^3 g(T_h-T_c)}{\eta\nu}$, $Re=\frac{U_0 L_0}{\nu}$, and $Pr=\frac{\nu}{\eta}$, where g is the gravitational acceleration and $\nu(=\frac{\mu}{\rho_0})$ the kinematic viscosity. In homogeneous fluids, unlike mixed convection, Iwatsu et al. [21], there is no reference scale velocity inherent in problems of natural (or free) convection; then, defining $U=\frac{\nu}{L_0}$ implies $Re=1$, Gunzburger [18, p. 218], Fig. 1 shows the 2D physical models to be considered.

The systems must be supplemented with initial conditions $\mathbf{u}(\mathbf{x},0)=\mathbf{u}_0(\mathbf{x})$ and $\theta(\mathbf{x},0)=\theta_0(\mathbf{x})$ in Ω; and boundary conditions, for instance $\mathbf{u}=\mathbf{f}$ and $B\theta=0$ on Γ, $t\geqslant 0$, where B is a temperature boundary operator that can involve Dirichlet, Neumann or mixed boundary conditions.

Restricting systems (1)–(3) and (4)–(6) to a two-dimensional region Ω, applying the curl in both sides of the momentum equations, and considering that $\nabla\cdot\mathbf{u}=0$ implies the existence of a function ψ, called the stream function, such that

$$u_1=\frac{\partial\psi}{\partial y},\quad u_2=-\frac{\partial\psi}{\partial x} \tag{7}$$

where $(u_1,u_2)=\mathbf{u}$; then, the following scalar systems are obtained, the unitary vector **e** has been replaced by the angle of inclination ϕ of the region Ω through $\mathbf{e}=(\sin\phi,\cos\phi)$, in Ω, $t>0$

(pm):

$$\nabla^2\psi=Ra_p\left(\frac{\partial\theta}{\partial x}\cos\phi-\frac{\partial\theta}{\partial y}\sin\phi\right) \tag{8}$$

$$\theta_t-\nabla^2\theta+\mathbf{u}\cdot\nabla\theta=0, \tag{9}$$

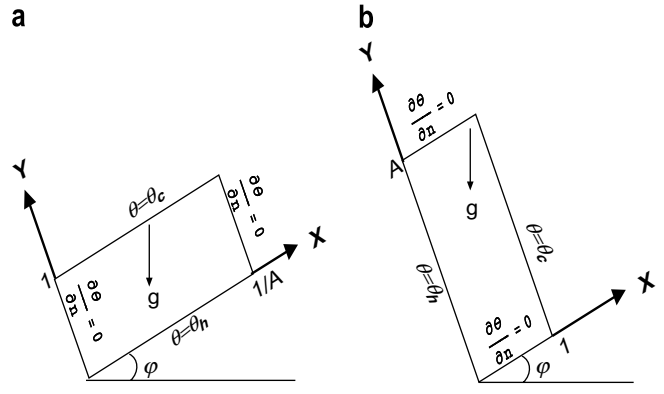

Fig. 1. 2D physical models: (a) porous media and (b) homogeneous fluid.

(hf):

$$\nabla^2\psi=-\omega \tag{10}$$

$$\omega_t-\nabla^2\omega+\mathbf{u}\cdot\nabla\omega=\frac{Ra_h}{Pr}\left(\frac{\partial\theta}{\partial x}\cos\phi-\frac{\partial\theta}{\partial y}\sin\phi\right) \tag{11}$$

$$\theta_t-\gamma\nabla^2\theta+\mathbf{u}\cdot\nabla\theta=0 \tag{12}$$

where the vorticity ω is given by $\omega=\frac{\partial u_2}{\partial x}-\frac{\partial u_1}{\partial y}$, from $\omega\mathbf{k}=\nabla\times\mathbf{u}=-\nabla^2\psi\mathbf{k}$. It should be noted that $\gamma=1/Pr$ and $Re=1$ have been replaced. Both systems represent the Boussinesq approximation in ψ and ω variables of systems (1)–(3) and (4)–(6).

Denoting with a the width of a bi-dimensional cavity and with b its height, for homogeneous fluid an alternative dimensionless system similar to (4)–(6) can be obtained if $L_0=a$, $U_0=\sqrt{g\beta a\Delta T}$, and $T_0=\frac{T_h+T_c}{2}$ are considered; where U_0 is a reference velocity depending on the temperature difference ΔT. Like before, once the rotational is applied, the corresponding alternative system in stream function-vorticity variables reads, in Ω, $t>0$

(hf):

$$\nabla^2\psi=-\omega \tag{13}$$

$$\omega_t-\sqrt{\frac{Pr}{Ra_h}}\nabla^2\omega+\mathbf{u}\cdot\nabla\omega=\left(\frac{\partial\theta}{\partial x}\cos\phi-\frac{\partial\theta}{\partial y}\sin\phi\right) \tag{14}$$

$$\theta_t-\frac{1}{\sqrt{Ra_h Pr}}\nabla^2\theta+\mathbf{u}\cdot\nabla\theta=0 \tag{15}$$

The flow in a cavity where the side-walls are at constant but with different temperatures is to great extent determined by the value of Ra_h. For low values of Ra_h the dimensionless system of equations given by (4)–(6), (10)–(12) is appropriated but when this value is rather large the alternative system (13)–(15) is more suitable.

The pressure has been eliminated since the curl of the gradient is zero and the incompressibility condition is satisfied automatically, by (7). However, for homogeneous fluids one has the inconvenience that there is no boundary condition for ω and a procedure must be given to construct it.

This work is concerned with natural convection in rectangular cavities, then the equations are set in $\Omega=(0,a)\times(0,b)$; $a>0$, $b>0$. For viscous fluids $\mathbf{u}=\mathbf{0}$ on solid walls; in natural convection all the walls of the cavities are solid, then by (7). ψ is constant and it can be chosen to be 0. To construct the boundary condition for ω various alternatives have been proposed, see for instance Dean et al. [22], Peyret and Taylor [23]. Here the alternative in Nicolás and Bermúdez [24], extended to natural convection problems in rectangular cavities, is used: by Taylor expansion of ψ on the boundary and using (10), the following $O(h_x^2)$ (the first two) and $O(h_y^2)$ (the last two) relations are obtained

$$\omega(0,y,t)=-\frac{1}{2h_x^2}[8\psi(h_x,y,t)-\psi(2h_x,y,t)] \tag{16a}$$

$$\omega(a,y,t)=-\frac{1}{2h_x^2}[8\psi(a-h_x,y,t)-\psi(a-2h_x,y,t)] \tag{16b}$$

$$\omega(x,0,t) = -\frac{1}{2h_y^2}[8\psi(x,h_y,t) - \psi(x,2h_y,t)] \tag{16c}$$

$$\omega(x,b,t) = -\frac{1}{2h_y^2}[8\psi(x,b-h_y,t) - \psi(x,b-2h_y,t)] \tag{16d}$$

where h_x and h_y denote the size of the spatial discretization in X and Y directions.

The local Nusselt number Nu measures the heat transfer at each point on the wall where the temperature is specified and the global Nusselt number $\overline{Nu}$ measures the total rate of heat transfer on the wall. These non-dimensional parameters are defined by

Local Nusselt number:

$$Nu(x) = \left|\frac{a}{b}\frac{\partial\theta}{\partial y}\right|_{y=0,b} \quad \text{or} \quad Nu(y) = \left|\frac{b}{a}\frac{\partial\theta}{\partial x}\right|_{x=0,a}$$

Global Nusselt number:

$$\overline{Nu}|_{y=0,b} = \int_0^a Nu(x)\,\mathrm{d}x \quad \text{or} \quad \overline{Nu}|_{x=0,a} = \int_0^b Nu(y)\,\mathrm{d}y$$

3. Numerical method

The time derivatives ω_t, θ_t in systems (8)–(12), and (13)–(15) are approximated by

$$f_t(\mathbf{x},(n+1)\Delta t) \approx \frac{3f^{n+1} - 4f^n + f^{n-1}}{2\Delta t} \tag{17}$$

where $n \geqslant 1$, $\mathbf{x} \in \Omega$, $\Delta t > 0$ is the time step, f^r is an approximation of $f(\mathbf{x}, r\Delta t)$. It is known that (17) is a second order approximation for sufficiently smooth function f.

Once (17) is applied on ω_t, θ_t the following systems are obtained in Ω, incorporating the boundary condition on Γ for ψ, θ, and ω as discussed before; the detail for (13)–(15) is skipped,

(pm):

$$\nabla^2\psi^{n+1} = Ra_{\mathrm{p}}\left(\frac{\partial\theta^{n+1}}{\partial x}\cos\phi - \frac{\partial\theta^{n+1}}{\partial y}\sin\phi\right), \quad \psi^{n+1}|_\Gamma = 0 \tag{18}$$

$$\alpha\theta^{n+1} - \nabla^2\theta^{n+1} + \mathbf{u}^{n+1}\cdot\nabla\theta^{n+1} = f_\theta, \quad B\theta^{n+1}|_\Gamma = 0 \tag{19}$$

(hf):

$$\nabla^2\psi^{n+1} = -\omega^{n+1}, \quad \psi^{n+1}|_\Gamma = 0 \tag{20}$$

$$\alpha\omega^{n+1} - \nabla^2\omega^{n+1} + \mathbf{u}^{n+1}\cdot\nabla\omega^{n+1} = \frac{Ra_{\mathrm{h}}}{Pr}\left(\frac{\partial\theta^{n+1}}{\partial x}\cos\phi - \frac{\partial\theta^{n+1}}{\partial y}\sin\phi\right) + f_\omega, \quad \omega^{n+1}|_\Gamma = \omega_{bc}^{n+1} \tag{21}$$

$$\alpha\theta^{n+1} - \gamma\nabla^2\theta^{n+1} + \mathbf{u}^{n+1}\cdot\nabla\theta^{n+1} = f_\theta, \quad B\theta^{n+1}|_\Gamma = 0 \tag{22}$$

where $\alpha = \frac{3}{2\Delta t}$, $f_w = \frac{4w^n - w^{n-1}}{2\Delta t}$, $f_\theta = \frac{4\theta^n - \theta^{n-1}}{2\Delta t}$, $\mathbf{u}$ in terms of ψ is given by (7), ω_{bc} denotes the ω boundary condition in (16) and B the θ boundary operator.

Renaming $(\omega^{n+1},\theta^{n+1},\psi^{n+1})$ by (ω,θ,ψ) to simplify the notation, we must solve at each time level, for (20)–(22), a non-linear elliptic system of the form

(hf):

$$\nabla^2\psi = -\omega, \quad \psi|_\Gamma = 0 \tag{23}$$

$$\alpha\omega - \nabla^2\omega + \mathbf{u}\cdot\nabla\omega = \frac{Ra_{\mathrm{h}}}{Pr}\left(\frac{\partial\theta}{\partial x}\cos\phi - \frac{\partial\theta}{\partial y}\sin\phi\right) + f_\omega, \quad \omega|_\Gamma = \omega_{bc} \tag{24}$$

$$\alpha\theta - \gamma\nabla^2\theta + \mathbf{u}\cdot\nabla\theta = f_\theta, \quad B\theta|_\Gamma = 0 \tag{25}$$

and a similar one for (18) and (19). To obtain $(\omega^1,\theta^1,\psi^1)$ in (18) and (19) and (20)–(22), a first order approximation is applied in the temporal derivatives through a subsequence with a smaller time step to maintain second order precision; elliptic systems like the one in (23)–(25) are also obtained.

Denoting by

$$\Theta(\psi,\theta) \equiv (\alpha I - \varsigma\nabla^2)\theta + \mathbf{u}\cdot\nabla\theta - f_\theta$$

where ς is 1 for (19) and γ for (22) (or (25)), and by

$$W(\psi,\theta,\omega) \equiv \alpha\omega - \nabla^2\omega + \mathbf{u}\cdot\nabla\omega - \frac{Ra_{\mathrm{h}}}{Pr}\left(\frac{\partial\theta}{\partial x}\cos\phi - \frac{\partial\theta}{\partial y}\sin\phi\right) - f_\omega$$

then, system (23)–(25) and the analogous for (18) and (19) are equivalent to

(pm):

$$\nabla^2\psi = Ra_{\mathrm{p}}\left(\frac{\partial\theta}{\partial x}\cos\phi - \frac{\partial\theta}{\partial y}\sin\phi\right), \quad \psi|_\Gamma = 0 \tag{26}$$

$$\Theta(\psi,\theta) = 0, \quad B\theta|_\Gamma = 0 \tag{27}$$

(hf):

$$\nabla^2\psi = -w, \quad \psi|_\Gamma = 0 \tag{28}$$

$$W(\psi,\theta,\omega) = 0, \quad \omega|_\Gamma = \omega_{bc} \tag{29}$$

$$\Theta(\psi,\theta) = 0, \quad B\theta|_\Gamma = 0 \tag{30}$$

These systems are solved with the following fixed point iterative process

(hf):

Given $(\theta^0,\omega^0) = (\theta^n,\omega^n)$, with $\lambda > 0$, solve until convergence on θ and ω

$$\nabla^2\psi^{m+1} = -\omega^m, \quad \psi^{m+1}|_\Gamma = 0 \tag{31}$$

$$\theta^{m+1} = \theta^m - \lambda(\alpha I - \gamma\nabla^2)^{-1}\Theta(\psi^{m+1},\theta^m), \quad B\theta^{m+1}|_\Gamma = 0 \tag{32}$$

$$\omega^{m+1} = \omega^m - \lambda(\alpha I - \nabla^2)^{-1}W(\psi^{m+1},\theta^{m+1},\omega^m), \quad \omega^{m+1}|_\Gamma = \omega_{bc}^m \tag{33}$$

and take

$$(\psi^{n+1},\theta^{n+1},\omega^{n+1}) = (\psi^{m+1},\theta^{m+1},\omega^{m+1})$$

for (28)–(30), and one similar for (26) and (27):

"Given $\theta^0 = \theta^n$ solve until convergence on $\theta\ldots$, and take $(\psi^{n+1},\theta^{n+1}) = (\psi^{m+1},\theta^{m+1})$".

The partial differential equation problem for θ^{m+1} in both systems is equivalent to

$$(\alpha I - \nabla^2)\theta^{m+1} = (\alpha I - \varsigma\nabla^2)\theta^m - \lambda\Theta(\psi^{m+1},\theta^m), \quad B\theta^{m+1}|_\Gamma = 0$$

and the one for ω^{m+1} in (33) to

$$(\alpha I - \nabla^2)\omega^{m+1} = (\alpha I - \nabla^2)\omega^m - \lambda W(\psi^{m+1}, \theta^{m+1}, \omega^m),$$
$$\omega^{m+1}|_\Gamma = \omega^m_{bc}$$

Therefore, at each iteration of each time level, uncoupled symmetric elliptic linear problems associated with the operators ∇^2, $\alpha I - \varsigma\nabla^2$, and $\alpha I - \nabla^2$ must be solved. For homogeneous fluids the iterative process is extended until the boundary to be able to construct the boundary condition for ω in (16) given implicitly in terms of ψ in Ω.

For the elliptic problems above very efficient solvers exist regardless of the space discretization. The results of this work are obtained with the second order approximation of the Fishpack solver [25], where the algebraic linear systems are solved with an efficient cyclic reduction iterative method [26]. As already mentioned, the first time derivatives are approximated with the second order one in (17) whereas the first space derivatives of ψ in (7) to obtain $\mathbf{u}$ in (8)–(12) and (13)–(15), the normal derivative of the boundary condition for θ, described later on, and the first space derivatives for the local Nusselt number are approximated by the centered second order finite difference approximation in interior points and by (17) in boundary points; to approximate the integral in the global Nusselt number the second order trapezoid rule (in the entire interval) is used. These second order approximations, complemented with the second order one of the boundary condition for ω in (16) for the elliptic problems, imply that the whole problem relies on second-order approximations.

4. Results and discussion

The initial condition for temperature and vorticity are given by $\theta(\mathbf{x},0) = 0$ and $\omega(\mathbf{x},0) = 0$. The parameter λ in the iterative process is chosen as $\lambda = 0.7$ and the stopping absolute criterion for the iterative process as 10^{-5}. For porous media the Rayleigh number considered lies in the range $60 \leqslant Ra_p \leqslant 10^4$ while for homogeneous fluids lies in $10^4 \leqslant Ra_h \leqslant 10^6$ and $Pr = 0.71$ which means that the cavity is filled with air. The results are reported through the streamlines of the stream function and the isotherms of the temperature; the iso-contours values, unless the contrary should be stated, are default ones. The aspect ratio A, the angle ϕ, the boundary condition for temperature (contained so far in the operator B) and the discretization parameters, time step Δt and the size of the mesh $h_x \times h_y$, will be specified in each case under study.

Unless the contrary should be indicated, the results shown correspond to steady state flows from the unsteady problem. They are the converged asymptotic steady state as time t approaches $+\infty$ (large time, in practice). To reach convergence to an asymptotic steady state a stopping criterion must be given for the final time T_{ss} when it occurs. Since T_{ss} is the time when the solution does not change any more with respect to time at any spatial point occupied by the fluid, Nicolás and Bermúdez [27], T_{ss} is determined with the point-wise discrete L_∞ absolute criterion in the closure $\overline{\Omega}$ of the cavity

$$\omega : \|\omega^{n+1}_{hx,hy} - \omega^n_{hx,hy}\|_\infty$$
$$\theta : \|\theta^{n+1}_{hx,hy} - \theta^n_{hx,hy}\|_\infty$$

Firstly, numerical experiments are reported to validate the numerical scheme with well-known results supposed to be correct. Secondly, new results are presented which to support they are correct a time step and mesh independence studies with the point-wise discrete L_∞ relative error in $\overline{\Omega}$

$$\Delta t \text{ fixed: } \frac{\|f_{hx1,hy1;\Delta t} - f_{hx2,hy2;\Delta t}\|_\infty}{\|f_{hx1,hy1;\Delta t}\|_\infty}$$
$$\{h_x, h_y\} \text{ fixed: } \frac{\|f_{hx,hy;\Delta t1} - f_{hx,hy;\Delta t2}\|_\infty}{\|f_{hx,hy;\Delta t1}\|_\infty}$$

are made. All the results are complemented with their local Nu and global $\overline{Nu}$ Nusselt numbers and the extreme values of the stream function ψ.

4.1. Porous media

4.1.1. Tilted horizontal cavities

The boundary condition for the temperature is given by

$$\frac{\partial\theta}{\partial n}|_{x=0,1} = 0, \quad \theta|_{y=0} = 1, \quad \theta|_{y=1} = 0$$

Lateral walls are adiabatic and horizontal walls with specified constant temperature, then heating occurs on the lower wall. It should be noted that the problem is re-scaled in order to x and y vary from $0 < x, y < 1$ then for a given aspect ratio A the one considered here is $D = 1/A = \frac{a}{b}$, which must appear explicitly in the respective equations. Various values of the Rayleigh number Ra_p, h_x, h_y, Δt, D and the angle ϕ with $0° \leqslant \phi \leqslant 180°$ are considered. Single or multiple cells appear depending on the value of these parameters.

Results for $Ra_p = 10^2$ with some aspect ratios and angles are shown on Table 1. The maximum value of the stream function ψ_{max} increases with the angle but the global Nusselt number $\overline{Nu}$ oscillates. Further experiments, not reported here, for $Ra_p \geqslant 60$, $D > 1$ fixed, and angles $0 \leqslant \phi \leqslant 180$, indicate, like in Moya et al. [1], that $\overline{Nu}$, as function of the angle, has two local maxima: one when multiple cells appear and the other when a single cell is obtained.

Table 1
Results with $Ra_p = 10^2$ and $\Delta t = 2 \times 10^{-3}$

D	$h_x \times h_y$	ϕ	ψ_{max}	$\overline{Nu}$	Number of cells	T_{ss}
3	1/60 × 1/40	10°	2.0409	2.8663	3	0.212
		25°	2.3956	2.2494	1 + sec.	0.168
		40°	2.8887	2.5491	1	0.338
10	1/100 × 1/20	10°	0.5860	2.7302	13	0.724
		40°	0.8480	1.5218	1 + sec.	0.472
		55°	1.0237	1.6240	1	0.452

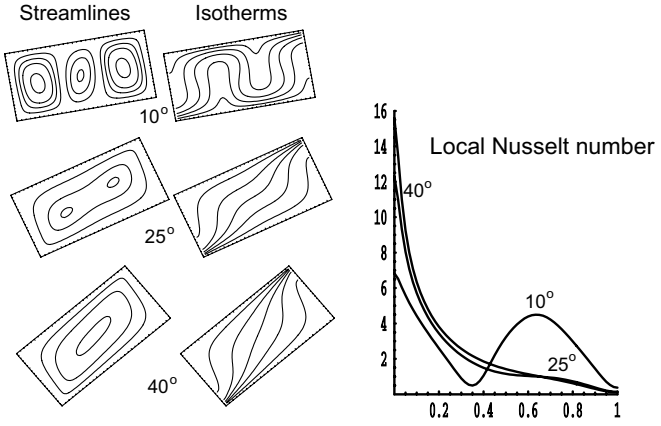

Fig. 2. $Ra_p = 10^2$, $D = 3$, $\Delta t = 2 \times 10^{-3}$ and $h_x \times h_y = \frac{1}{60} \times \frac{1}{40}$.

Fig. 2 shows streamlines, isotherms and local Nusselt number on the bottom wall, for $Ra_p = 10^2$, $D = 3$, and three angles. When $\phi = 40°$ the streamlines show that the hot fluid on the bottom rises near the right wall until the top cold wall and turns to fall on the left side forming a counterclockwise rotating cell; on the other hand, different isotherms lie closer each other in the left corner than in other part on the hot wall, which indicates more vertical variation of the temperature and therefore the local Nusselt number on the bottom hot wall has only one maximum near the left corner and one minimum in the right one. When the angle diminishes to $\phi = 25°$, secondary cells appear. When $\phi = 10°$ three cells rotating in opposite directions each other are obtained; different isothermals on the bottom wall are close each other in the left corner but near the center also, that is, in the limit between cells where the fluid comes from the cold to the hot wall, hence there are two places on the bottom where exist more heat transfer, and then, the local Nusselt number has two maxima and two minima.

Something similar occurs with $D = 10$ but the number of convective cells for small angles is 13 which shows that heat transfer has been increased in more places than for $D = 3$ implying that the local Nusselt number has now seven maxima and equal number of minima. However, from Table 1 it is observed that the global Nusselt number $\overline{Nu}$ decreases when the aspect ratio increases, regardless of the angle. Results with $D = 3$ are in agreement with those reported by Moya et al. [1] but for $D = 10$ they report only nine cells and hence less than seven maxima and seven minima for the local Nusselt number while in this work various meshes and time step sizes showed that different quantity of cells can be obtained depending on the size of the mesh: nine cells with a square mesh $\frac{1}{30} \times \frac{1}{30}$ until 15 with a finer horizontal mesh $\frac{1}{400} \times \frac{1}{40}$.

Denoting by ϕ_s the transition angle, with $0° \leqslant \phi < \phi_s$, to pass from multiple cells to a single cell, analysis for $Ra_p = 10^2$ with various mesh sizes, time steps, and other aspect ratios was made to figure it out ϕ_s, Table 2. It is observed that with $D = 4$, $D = 8$, and $D = 10$ the angles

Table 2
Angles of transition for $Ra_p = 10^2$ and various aspect ratios

D	ϕ_s (transition)
2	11°
3	24°
4	29°
8	32°
10	30°

differ among them by little while with $D = 3$, and mainly with $D = 2$, there is a noticeable difference. These angles are the same of those in Moya et al. [1] except for aspect ratios 2 and 3 where the discrepancies are of 1° only.

Going further than in Moya et al. [1], experiments for the higher Rayleigh number $Ra_p = 10^3$ with the same aspect ratios are studied, to the best of our knowledge this is the first time they are reported. To validate these new flows with $D = 3$, computations were made for three mesh sizes and three time steps, considering $\phi = 0°$:

(1) time step fixed $\Delta t = 10^{-5}$ and $(h_x, h_y) = (1/150, 1/50)$, $(1/225, 1/75)$, $(1/300, 1/100)$;
(2) mesh size fixed $(h_x, h_y) = (1/225, 1/75)$ and $\Delta t = 10^{-5}$, 5×10^{-6}, 2.5×10^{-6}.

The discrepancies for each set of computations are:

(1) at most 4.4% (4.4% for stream function and 1.5% for temperature);
(2) at most 1.1% (1.1% for stream function and less than 0.3% for temperature).

The correspondent max/min values of stream function ψ in each case are:

(1) max/min = 11.6464/−16.9201, 11.7949/−16.6909, 11.8455/−16.6041, respectively;
(2) max/min = 11.7949/−16.6909, 11.8391/−16.6627, 11.9054/−16.6190, respectively.

Therefore, due to the above discrepancies and since there are no changes with finer meshes, the result shown in Fig. 3 is taken as the correct one.

It is observed in Fig. 3 that qualitatively for $Ra_p = 10^3$ occurs something similar for $Ra_p = 10^2$: multiple cells are obtained in the streamlines for the smallest angle $\phi = 10°$; with $\phi = 25°$ one main cell and two secondary cells appear; for $\phi = 40°$ only one main cell appears as in $Ra_p = 10^2$. However, some differences can be observed; the isotherms and the cells of the streamlines appear distorted with small angles and more than three convective cells are obtained with $\phi = 10°$, and with $\phi = 25°$ the secondary cells are larger and each one fills almost half of the cavity, the respective local Nusselt numbers show that although the majority of the heat transfer occurs in the left corner, when $\phi = 10°$ there exists other maximum near the

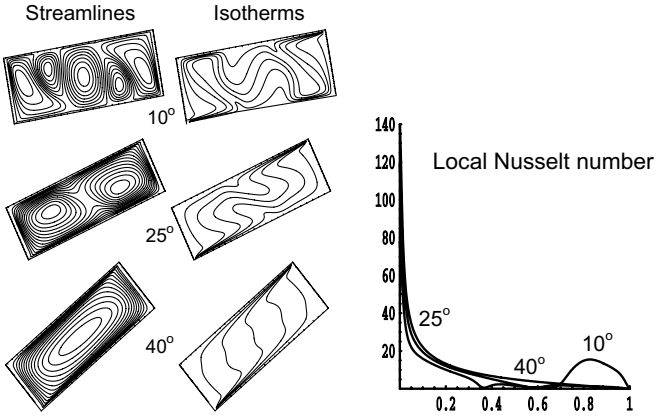

Fig. 3. $Ra_p = 10^3$, $D = 3$, $\Delta t = 10^{-5}$ and $h_x \times h_y = \frac{1}{225} \times \frac{1}{75}$.

right corner and this seems a consequence that the small cell near the right wall picks heat from the hot to the cold wall.

Table 3 shows some results with $D = 3$ and $D = 10$ with suitable meshes. It is noticed that ψ_{max} and $\overline{Nu}$ have increased with respect to $Ra_p = 10^2$, see Table 1, which indicate stronger motion and in consequence higher heat transfer; however for $Ra_p = 10^3$ fixed those values diminished if the aspect ratio D increases and both show to be functions of the angle ϕ. For $D = 3$, the angle of transition $\phi_s = 24°$ equals the one for $Ra_p = 10^2$ but for $D = 10$ the angle $\phi_s = 27°$ is smaller than the one for $Ra_p = 10^2$.

For $Ra_p = 10^2$ with several aspect ratios and angles, Table 4 shows a comparison of some values of the heat transfer, through the global Nusselt number $\overline{Nu}$, and the number of cells obtained in this work, values indicated by (B), with those in Caltagirone and Bories [28], values indicated by (C). It is observed that the difference between the respective values of $\overline{Nu}$ is less than 9% in all cases but the number of cells can be different.

Table 3
Results with $Ra_p = 10^3$ and $\Delta t = 10^{-5}$

D	$h_x \times h_y$	ϕ	ψ_{max}	$\overline{Nu}$	Number of cells	T_{ss}
3	1/225 × 1/75	10°	16.8320	8.7687	5	0.00931
		25°	17.5419	8.0889	1 + sec.	0.01011
		40°	16.4969	9.9158	1	0.01312
10	1/500 × 1/50	10°	3.9961	3.6459	5 + sec	0.00956
		40°	7.0677	4.5745	1 + sec.	0.03087
		55°	7.4627	5.2531	1	0.03007

Table 4
Global Nusselt number for $Ra_p = 10^2$ and $\Delta t = 2 \times 10^{-3}$

D	ϕ	$\overline{Nu}$ (C)	Number of cells (C)	$\overline{Nu}$ (B)	Number of cells (B)	Difference in $\overline{Nu}$ (%)
2	0°	2.65	3	2.70	3	2
	10°	2.60	3	2.38	1 + sec.	9
	15°	2.44	1	2.57	1	5
4	0°	2.67	5	2.75	5	3
	30°	2.57	1	2.37	1 + sec.	8
	40°	2.02	1	2.20	1	9
8	0°	2.64	11	2.70	11	2
	30°	2.45	4	2.25	1 + sec.	9
	40°	1.52	–	1.65	1	9

4.1.2. Tilted square and vertical cavities

In this case the temperature boundary condition is given by

$$\left.\frac{\partial\theta}{\partial y}\right|_{y=0,b} = 0, \quad \theta = 0.5, |_{x=0}, \quad \theta = -0.5|_{x=1}$$

Now horizontal walls are adiabatic and lateral ones with specified constant temperature, heating occurs on the left wall. It should be noted that this case is equivalent to the previous one, considering now that the vertical walls have specified temperature and the cavity is rotated 90°. Similar results are obtained as those in 4.1.1 for square and horizontal cavities for $Ra_p = 10^2$ since the configurations are the same: lateral walls become to be adiabatic and the bottom and top ones become with specified temperature, hot and cold respectively. Despite the temperature on these parts of the boundary is not the same as in the earlier case, the difference $\Delta\theta = 1$, which must be reflected in the results.

Results obtained for $Ra_p = 10^2$, 10^3, 10^4 and various angles showed to be in agreement with those in Baytas [3], from the unsteady problem. Fig. 4 shows streamlines and isotherms for $Ra_p = 10^4$ with some angles. With these angles one main cell appears in the streamlines and the central part of them and the one of the isotherms is extended toward the lateral walls with specified constant

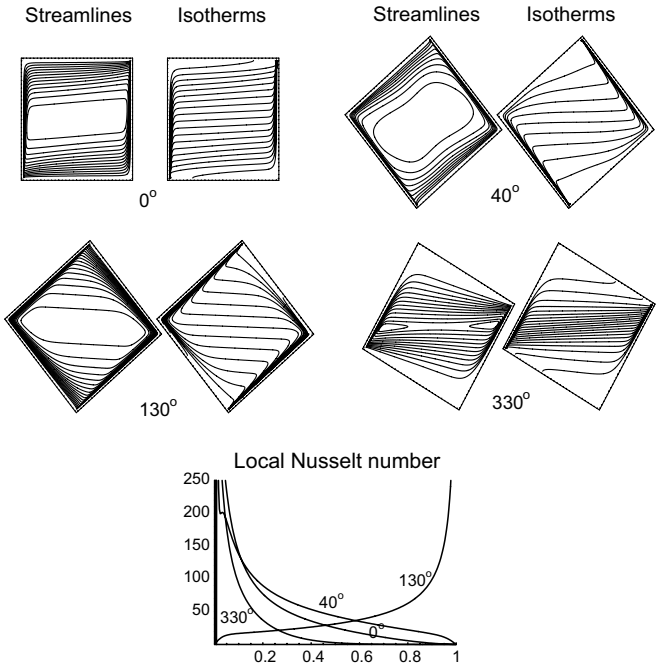

Fig. 4. $Ra_p = 10^4$, $A = 1$, $h_x \times h_y = 1/300 \times 1/300$ and $\Delta t = 2 \times 10^{-7}$.

temperature; streamlines and isotherms tend to adhere into those walls also. Stretched secondary cells appear for $\phi = 330°$. The local Nusselt number on the hot lateral wall shows that the highest heat transfer occurs in the lower corner for angles of 0°, 40°, and 330° but when the angle is 130° such value occurs in the upper corner because of the opposite effect of the buoyancy force since with the angle 130° the hot wall will have an angle of 40° with respect to the horizontal, and as it had been mentioned in 4.1.1, the fluid tends to rise from the hot to the cold wall counterclockwise.

For $Ra_p = 10^4$, Table 5 summarizes the global Nusselt number, extreme values of stream function ψ_m, maximum in positive values or minimum in negative values, and the final time T_{ss} to reach the steady state. When $\phi = 40°$ there is noticeable faster clockwise motion of the fluid, as ψ_m indicates, which forces a considerable increase of the heat transfer $\overline{Nu}$.

As Ra_p increases a noticeable diminution on the mesh size and time step Δt is required. For instance, for $Ra_p = 10^3$ a mesh of $1/70 \times 1/70$ and $\Delta t = 2 \times 10^{-5}$ is enough but for $Ra_p = 10^4$ a mesh $1/300 \times 1/300$ and $\Delta t = 2 \times 10^{-7}$ are required.

This time going further than Baytas [3] new results are reported for $Ra_p = 10^2$, 10^3 on vertical cavities, $A \geqslant 1$, with angles $0° \leqslant \phi \leqslant 360°$. Single and multiple convective cells are found.

Results with $A = 3$ and $Ra_p = 10^3$ considering $\phi = 0°$ were validated with:

(1) time step fixed $\Delta t = 10^{-5}$ and $(h_x, h_y) = (1/50, 3/150)$, $(1/75, 3/225)$, $(1/100, 3/300)$;
(2) mesh size fixed $(h_x, h_y) = (1/75, 3/225)$ and $\Delta t = 10^{-5}$, 5×10^{-6}, 2.5×10^{-6}.

The respective discrepancies were:

(1) at most 2.7% (2.4% for stream function and 2.7% for temperature);
(2) less than 1×10^{-4}% (less than 7.7×10^{-5}% for stream function and 9.9×10^{-5}% for temperature).

The maximum for stream function was zero in all cases and the correspondent minimum in each case is

(1) min = −37.4366, −38.1144, −38.3791 respectively;
(2) min = −38.1144, −38.1152, −38.1164 respectively.

Then, due to the above discrepancies and that there are not noticeable changes with finer meshes, the results taken as correct are shown in Fig. 5.

Although in Fig. 5 for $Ra_p = 10^3$, the streamlines have only one cell for the same angles considered in Fig. 4, it was observed that for angles ϕ nearest to 90° there appear multiple convective cells (nine cells are obtained with $\phi = 0°$). Moreover, the results with $\phi = 130°$ in Fig. 5 are equivalent to those in Fig. 3 for $\phi = 40°$, as it was early mentioned; the distortion observed in Fig. 5 is a consequence of the aspect ratio, this congruence can be seen as an additional validation. In similar way the Nusselt number shows that when one cell appears the greatest heat transfer is reached at the bottom while the lowest at the top with angles 0°, 40°, and 330° with opposite situation for 130° because of the reverse effect of the buoyancy. Table 6 shows the extremum values

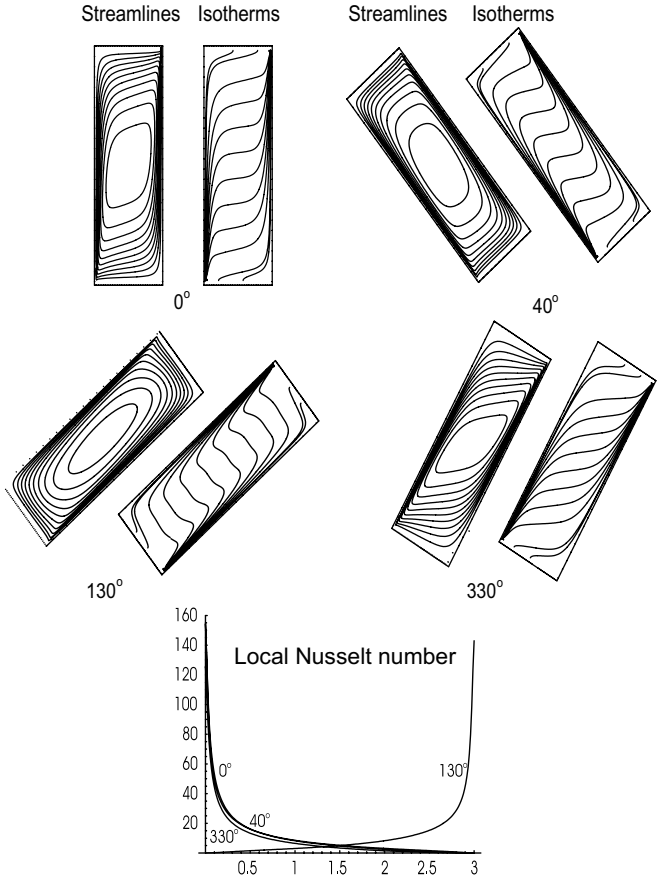

Fig. 5. $Ra_p = 10^3$, $A = 3$, $\Delta t = 10^{-5}$ and $h_x \times h_y = 1/75 \times 3/225$.

Table 5
Results for $Ra_p = 10^4$ with $A = 1$, $\Delta t = 2 \times 10^{-7}$ and $h_x \times h_y = 1/300 \times 1/300$

ϕ	ψ_m	$\overline{Nu}$	T_{ss}
0°	−69.2383	59.5447	0.015575
40°	−96.7505	150.3877	0.0009918
130°	87.1717	53.4990	0.0189956
330°	−36.6366	33.7527	0.0283764

Table 6
Results for $Ra_p = 10^3$ with $A = 3$, $\Delta t = 10^{-5}$ and $h_x \times h_y = 1/75 \times 3/225$

ϕ	ψ_m	$\overline{Nu}$	T_{ss}
0°	−38.1144	10.5268	0.02349
40°	−39.6460	10.5991	0.01996
130°	44.6996	9.9944	0.01530
330°	−30.5517	8.4037	0.11395

of the stream function ψ_m, and the global Nusselt number, the steady state times T_{ss}; with those angles a stronger counterclockwise motion is obtained with 130°, and the heat transfer is highest with 40°.

4.2. Homogeneous fluid

In Section 4.2.1 that follows computations are based on system (10)–(12) whereas those in Section 4.2.2, on system (13)–(15).

4.2.1. Tilted square cavity

Boundary condition for temperature, like in Section 4.1.2:

$$\frac{\partial\theta}{\partial y}\Big|_{y=0,1} = 0, \quad \theta = 0.5|_{x=0}, \quad \theta = -0.5|_{x=1}.$$

Computations were made on a mesh $h_x \times h_y = 1/30 \times 1/30$ and $\Delta t = 10^{-4}$ independently of the Rayleigh number Ra_h. Results for $Ra_h \leqslant 10^3$ show isothermals almost parallels to the lateral walls, one cell for the streamlines is obtained, and there exist small differences with the values of $\overline{Nu}$ and those of the extremum values of ψ regardless of the angle. For $Ra_h \geqslant 10^4$ changes in isothermals appear, they are not longer parallels, but one central cell is also obtained in streamlines.

Results for $Ra_h = 10^5$ and some angles are shown in Fig. 6. It is observed that the fluid motion is stronger. One main convective cell with secondary cells is obtained with some angles. With angles of 0°, 40°, and 330° the main cell rotates clockwise whereas with 130° rotates counterclockwise. On the hot wall the maximum of the local Nusselt number occurs near the lower corner with angles 0°, 40°, and 330°, and near the upper one with 130°; the curve decreases softly from the upper corner and reverse situation occurs with 130°.

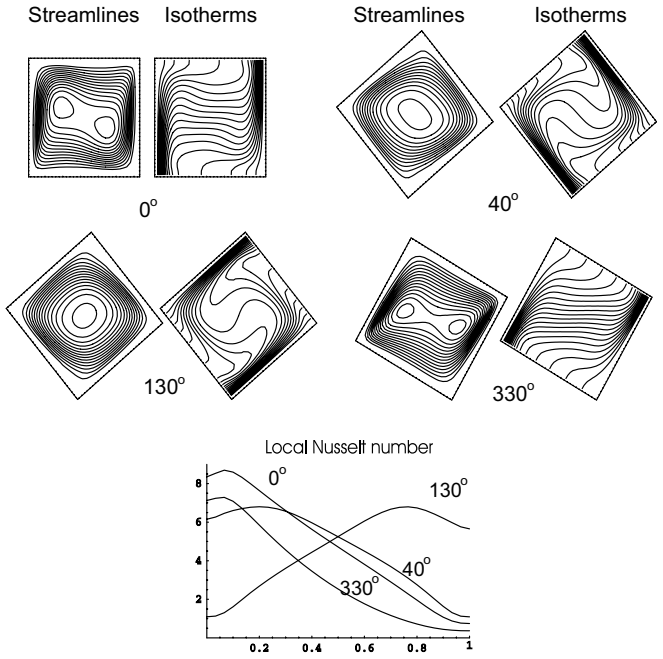

Fig. 6. $Ra_h = 10^5$, $A = 1$, $\Delta t = 10^{-4}$ and $h_x \times h_y = 1/30 \times 1/30$.

Table 7
Results for $Ra_h = 10^5$ and $Ra_h = 10^6$, with $A = 1$, $\Delta t = 10^{-4}$, $h_x \times h_y = 1/30 \times 1/30$

Ra_h	ϕ	ψ_m	$\overline{Nu}$	T_{ss}
10^5	0°	−13.4661	4.7504	0.2175
	40°	−24.6617	4.7386	0.2426
	130°	28.7379	4.6638	0.2843
	330°	−7.2228	3.1358	0.2386
10^6	0°	−23.8098	11.3083	0.1806
	40°	−41.8493	10.4157	0.2961
	130°	47.3883	9.9411	0.7188
	330°	−12.6913	6.5755	0.1977

In Table 7, results of the global Nusselt numbers, extremum values of the stream function, and the final times T_{ss} to reach steady state are shown for $Ra_h = 10^5$ and $Ra_h = 10^6$. It is observed that the fluid motion is stronger when Ra_h increases, as indicated by the extremum values of the stream function. Moreover, for both values of Ra_h the flow is faster when the angle is 130°, and more heat transfer is obtained in both cases when the angle decreases.

To validate the flow for $Ra_h = 10^6$ with our numerical method, computations were made with three mesh sizes and three different time steps, considering $\phi = 0°$:

(1) time step fixed, $\Delta t = 10^{-4}$ and $(h_x, h_y) = (1/30, 1/30)$, $(1/45, 1/45)$, $(1/60, 1/60)$;
(2) mesh size fixed $(h_x, h_y) = (1/30, 1/30)$ and $\Delta t = 10^{-4}$, 5×10^{-5}, 2.5×10^{-5}.

The discrepancies for each set of computations are:

(1) at most 7.7% (7.7% for vorticity, 2.2% for stream function and 5.4% for temperature);
(2) less than 1% (0.14% for vorticity, 0.13% for stream function and 0.08% for temperature).

The correspondent minimum values of stream function ψ in each case (the maximum value is always zero) are:

(1) min = −23.8070, −23.6150, −23.6034, respectively;
(2) min = −23.8070, −23.8043, −23.7993, respectively.

Due to the above discrepancies and because no change is observed in results with finer meshes, the flow in Fig. 7 is taken as the correct one. A more complex flow is observed. Two and three secondary cells may appear for some angles. Analogously as in porous media for $Ra_h = 10^4$, the central part of the streamlines is expanded and tends to adhere into the walls with specified temperature; for others angles it is extended toward all the walls. The corresponding local Nusselt number on the hot wall, shows a rapid descent close to the left lower corner. As observed, qualitatively the situation with $\phi = 130°$ is the opposite.

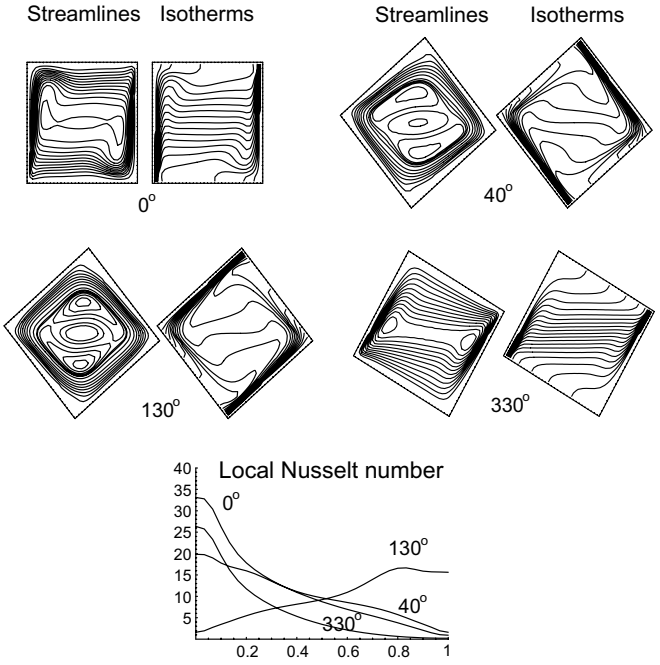

Fig. 7. $Ra_h = 10^6$, $A = 1$, $\Delta t = 10^{-4}$ and $h_x \times h_y = 1/30 \times 1/30$.

Table 8
Values of the global Nusselt and the maximum of the horizontal and vertical velocities for $\phi = 0°$ and $\Delta t = 10^{-4}$

Ra_h	$u_{1_{max}}$ (M)	$u_{2_{max}}$ (M)	$\overline{Nu}$ (M)	$u_{1_{max}}$ (B)	$u_{2_{max}}$ (B)	$\overline{Nu}$ (B)
10^3	3.54	3.59	1.108	5.081	5.140	1.117
10^4	16.18	19.44	2.201	22.513	27.017	2.257
10^5	42.51	69.08	4.430	58.773	91.990	4.750
10^6	117.8	226.7	8.754	172.644	295.914	9.245

Results for $Ra_h = 10^5$, 10^6 with angle $\phi = 0°$ are in agreement with those obtained by Bermúdez and Nicolás [12] and the ones for the inclined cavity for $Ra_h = 10^6$, with appropriated angles, agree with those obtained by Kuyper et al. [29] considering a square cavity heated from below.

For the global Nusselt number $\overline{Nu}$ on the hot wall and the maximum of the horizontal and vertical velocities $u_{1_{max}}$ and $u_{2_{max}}$ in all the cavity, Table 8 shows a comparison of the results obtained in this work, indicated by (B), with those obtained by Markatos and Pericleous [30], indicated by (M), from the steady problem. Important differences are noticed, mainly for values of the velocities; however, the results presented by Markatos an Pericleous were obtained without consider the Boussinesq approximation and they comment that some results of the Nusselt number with the Boussinesq approximation show differences up to 3.7% for $Ra_h = 10^5$ and 10^6.

4.2.2. Tall vertical cavity

Boundary conditions for temperature:

$$\frac{\partial \theta}{\partial y}|_{y=0,b} = 0, \quad \theta = 0.5|_{x=0}, \quad \theta = -0.5|_{x=1}.$$

Cavities without and with inclination are considered.

4.2.2.1. Untilted cavity.

Computational experiments in a vertical cavity without inclination and aspect ratio 8 were made for $Ra_h = 3.4 \times 10^5$ and 10^6. Results for the first value of Ra_h is reported in Glowinski [16] at some final times T's and our results agree with those. A mesh $h_x \times h_y = 1/30 \times 8/240$ and time step $\Delta t = 10^{-2}$ are used in all the experiments.

For both cases, more computations for larger times were made and they indicate that the flow is oscillatory, that is, it does not reach a steady state. Results at three different final times T are shown in Fig. 8 for $Ra_h = 3.4 \times 10^5$ and in Fig. 9 for $Ra_h = 10^6$. A large main cell with secondary cells, which appear larger for $Ra_h = 10^6$, is observed in the streamlines for both Ra_h. The respective local Nusselt number, at the three times, shows larger values for $Ra_h = 10^6$.

In Table 9, the global Nusselt number $\overline{Nu}$ shows also larger values for $Ra_h = 10^6$ although the magnitude of ψ_{min} indicates that the fluid motion is stronger for $Ra_h = 3.4 \times 10^5$ than $Ra_h = 10^6$ at $T = 150$ and $T = 500$. With Ra_h fixed, the global Nusselt number increases as the magnitude of ψ_{min} grows.

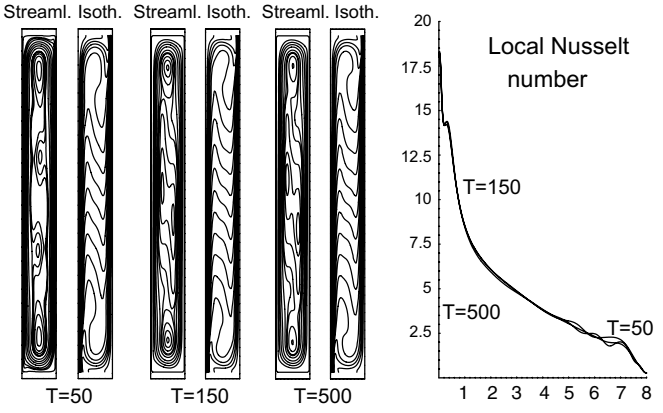

Fig. 8. $Ra_h = 3.4 \times 10^5$, $A = 8$, $\Delta t = 10^{-2}$ and $h_x \times h_y = 1/30 \times 8/240$.

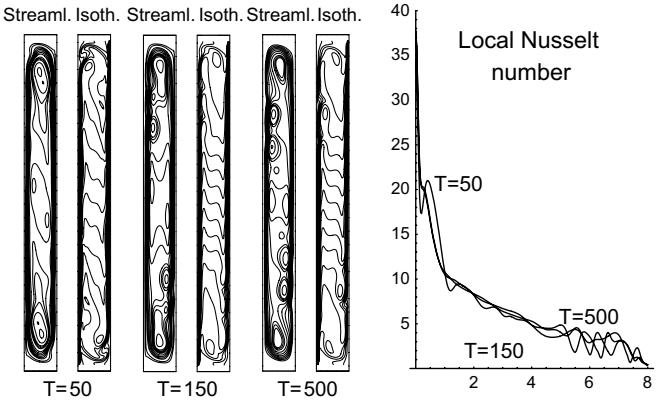

Fig. 9. $Ra_h = 10^6$, $A = 8$, $\Delta t = 10^{-2}$ and $h_x \times h_y = 1/30 \times 8/240$.

Table 9
Results for $Ra_h = 3.4 \times 10^5$ and $Ra_h = 10^6$ with $A = 8$, $\Delta t = 10^{-2}$ and $h_x \times h_y = 1/30 \times 8/240$ (untilted case)

Ra_h	ψ_{min}	$\overline{Nu}$	T
3.4×10^5	−0.1498	4.8471	50
	−0.1289	4.8354	150
	−0.1285	4.8352	500
10^6	−0.1737	6.6580	50
	−0.1097	6.5888	150
	−0.1207	6.6408	500

4.2.2.2. Tilted cavity. To observe the rotation effect of the vertical cavity on the fluid motion and on the heat transfer at fixed time, results with angles 40°, 130° and 330° are presented for $Ra_h = 3.4 \times 10^5$ and $T = 50$ in Fig. 10. The results with 0° can be seen in previous Fig. 8. To the best of our knowledge, these results are reported for the first time.

Table 10 summarizes the extremum values of the stream function and the global Nusselt number. It can be seen that the inclination of the cavity generates stronger fluid motion with certain angles, 40° and 130°, counterclockwise or clockwise, but the heat transfer $\overline{Nu}$ is higher without inclination, with the other angles it differs very little.

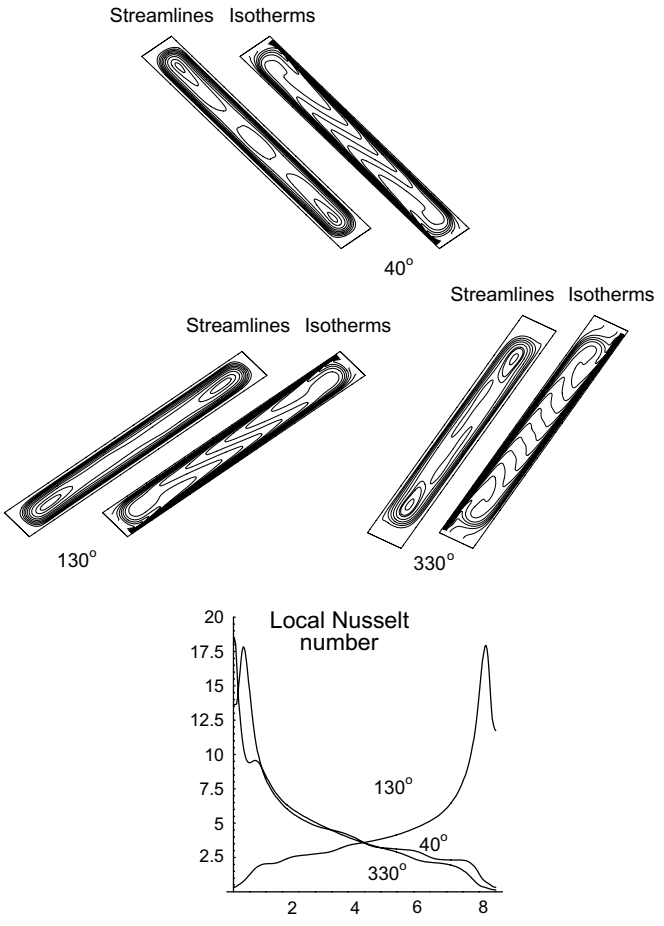

Fig. 10. $Ra_h = 3.4 \times 10^5$, $A = 8$, $\Delta t = 10^{-2}$, $T = 50$ and $h_x \times h_y = 1/30 \times 8/240$.

Table 10
Results for $Ra_h = 3.4 \times 10^5$ and $T = 50$ with $A = 8$, $\Delta t = 10^{-2}$ and $h_x \times h_y = 1/30 \times 8/240$ (tilted case)

ϕ	ψ_m	$\overline{Nu}$
0°	−0.1498	4.8471
40°	−0.1725	4.8046
130°	0.1745	4.6573
330°	−0.1325	4.3867

Finally, some similarities and discrepancies observed between porous media and homogeneous fluid are indicated.

Similarities :

(a) In both kind of fluid flow the fluid motion and the heat transfer are stronger in square cavities than in rectangular ones if the respective Rayleigh number is fixed,
(b) a more vigorous fluid motion is obtained when Ra_p or Ra_h increases implying higher heat transfer; however, this behavior may depend on the aspect ratio and on the angle of inclination,
(c) in square cavities, for $Ra_p \geqslant 10^3$ in porous media and $Ra_h \geqslant 10^5$ in homogeneous fluids one main cell appears but for some angles secondary cells appear and the isotherms and streamlines tend to adhere into the walls with specified temperature.

Discrepancies :

(a) The mesh size and the time step must be finer for porous media than for homogeneous fluids when Ra_p or Ra_h increases,
(b) in rectangular porous cavities with $Ra_p \geqslant 10^2$ there appears from one to multiple cells for some angles whereas in homogeneous fluids for Ra_h of the order of 10^5 and 10^6 in square and large enough vertical cavities one cell appears only, and at most secondary cells appear for some angles.

5. Conclusions

Results for porous media and homogeneous fluid, with a common structure in the numerical procedure, have been reported with a variety of situations on the Rayleigh number, aspect ratio and angle of inclination. The change of these parameters in porous media causes the necessity to use finer meshes and smaller time steps than in homogeneous fluid. For homogeneous fluid, at least with the stream function-vorticity variables, the situation is more relaxed because it is possible to obtain good results without refining too much the mesh size and the time step. The results strongly indicate that additional studies can be continued with the numerical procedure, specially those with

$A > 1$ for homogeneous fluid, in order to determine the kind of oscillatory flows for large times when they do not arrive toward a steady state, that is, to determine if the flow is periodic, quasi-periodic, or it involves a more complicated bifurcation structure. A study either on transient flows, like in Saeid and Pop [4] in porous media, or time-dependent plumes, Bastiaans et al. [31], extended to tilted rectangular cavities can be explored for homogeneous fluids. Moreover, in porous media, with some modifications of this numerical procedure, the case with variable porosity, Marcondes et al. [32], and variable anisotropy, Nguyen et al. [33], can be also explored as well as viscous effects near walls through the Brinkman extension, Rees [34]. About some specific findings in porous media: one rotating cell of the streamlines is always obtained for $Ra_p \leqslant 10^2$, $D = 1$, and $0° \leqslant \phi \leqslant 180°$; for $Ra_p \leqslant 10^2$ and $D \geqslant 2$ single or multiple cells are obtained depending on the angle ϕ. For $60 < Ra_p \leqslant 10^2$ and $D > 1$ the results show multiple cells, then the stream function has several extreme values for $0° \leqslant \phi < \phi_s$, with ϕ_s the angle where the transition to a single cell occurs implying that the stream function has one maximum only. Above ϕ_s a single cell always is obtained but if the angle ϕ is smaller than ϕ_s the unique maximum of the stream function starts to split into two parts. This means that although the whole body of fluid rotates in certain direction, small parts of fluid are isolated inside the main cell, and they rotate in the same direction of this main cell, around the extreme value, originating secondary cells. If ϕ reduces more, multiple cells appear and they rotate in opposite directions each other and therefore several extremum values for ψ are obtained.

Acknowledgement

We would like to thank the unknown reviewers for the careful reading of the manuscript and his remarks which have improved the presentation of this work.

References

[1] S.L. Moya, E. Ramos, S. Mihir, Numerical study of natural convection in a tilted rectangular porous material, Int. J. Heat Mass Transfer 30 (4) (1987) 741–756.
[2] Mihir Sen, P. Vasseur, L. Robillard, Multiple steady states for unicellular natural convection in an inclined porous layer, Int. J. Heat Mass Transfer 30 (10) (1987) 2097–2113.
[3] A.C. Baytas, Entropy generation for natural convection in a inclined porous cavity, Int. J. Heat Mass Transfer 43 (2000) 2089–2099.
[4] N.H. Saeid, I. Pop, Transient free convection in a square cavity filled with porous medium, Int. J. Heat Mass Transfer 47 (2004) 1917–1924.
[5] R. Bennacer, H. Beji, F. Oueslati, A. Belghith, Multiple natural convection solution in porous media under cross temperature and concentration gradients, Numer. Heat Transfer: Part A: Appl. 39 (6) (2001) 553–567.
[6] A.M. Al-Amiri, Nature convection in porous enclosures: the application of the two-energy equation model, Numer. Heat Transfer: Part A: Appl. 41 (8) (2002) 817–834.
[7] K. Slimi, L. Zili-Ghedira, S. Ben Nasrallah, A.A. Mohamad, A transient study of coupled natural convection and radiation in a porous vertical channel using the finite-volume method, Numer. Heat Transfer: Part A: Appl. 45 (5) (2004) 451–478.
[8] S. Das, Y.S. Morsi, A non-Darcian numerical modeling in domed enclosures filled with heat-generating porous media, Numer. Heat Transfer: Part A: Appl. 48 (2) (2005) 149–164.
[9] K. Slimi, M. Mhimid, M. Ben Salah, S. Ben Nasrallah, A.A. Mohamad, L. Storesletten, Anisotropy effects on heat and fluid flow by unsteady natural convection and radiation in saturated porous media, Numer. Heat Transfer: Part A: Appl. 48 (8) (2005) 763–790.
[10] F.J. Hamady, J.R. Lloyd, H.Q. Yang, K.T. Yang, Study of local natural convection heat transfer in an inclined enclosure, Int. J. Heat Mass Transfer 32 (9) (1989) 1697–1708.
[11] R.A.W.M. Henkes, C.J. Hoogendoorn, Scaling of laminar natural-convection flow in a heated square cavity, Int. J. Heat Mass Transfer 36 (11) (1993) 2913–2925.
[12] B. Bermúdez, A. Nicolás, An operator splitting numerical scheme for thermal/isothermal incompressible viscous flows, Int. J. Numer. Methods Fluids 29 (1999) 397–410.
[13] M.A. Christon, P.M. Gresho, S.B. Sutton, Special session computational predictability of natural convection flows in enclosures', in: First M.I.T. Conference on Computational Fluid and Solid Mechanics, Massachusetts Institute of Technology, Cambridge, Massachusetts, USA, June 2001.
[14] S. Xin, P. Le Quéré, An extended Chebyshev pseudo-spectral benchmark for the 8:1 differentially heated cavity, Int. J. Numer. Methods Fluids 40 (2002) 981–998.
[15] F. Auteri, N. Parolini, Numerical investigation of the first instabilities in the differentially heated 8:1 cavity, Int. J. Numer. Methods Fluids 40 (2002) 1121–1132.
[16] R. Glowinski, Handbook of Numerical Analysis: Numerical Methods for Fluids (Part 3), North-Holland, 2003.
[17] E. Báez, B. Bermúdez, A. Nicolás, Convección natural en medios porosos y libres: simulación numérica, Rev. Mex. De Física 50 (2004) 36–48.
[18] M.D. Gunzburger, Finite Element Methods for Viscous Incompressible Flows: A Guide to Theory, Practice, and Algorithms, Academic Press, Inc., 1989.
[19] L.D. Landau, E.M. Lifshitz, Fluid Mechanics, second ed., Pergamon Press, Inc., 1989.
[20] L.G. Leal, Laminar Flow and Convective Transport Processes, Series in Chemical Engineering, Butterworth-Heinemann, 1992.
[21] R. Iwatsu, Jae Min Hyn, Kunio Kuwahara, Mixed convection in a driven cavity with a stable vertical temperature gradient, Int. J. Heat Transfer 36 (1993) 1601–1608.
[22] E.J. Dean, R. Glowinski, O. Pironneau, Iterative solution of the stream function-vorticity formulation of the Stokes problem, applications to the numerical simulation of in compressible viscous flow, Comput. Methods Appl. Mech. Eng. 87 (1991) 117–155.
[23] R. Peyret, T.D. Taylor, Computational Methods for Fluid Flow, Springer-Verlag, New York, 1983.
[24] A. Nicolás, B. Bermúdez, 2D Incompressible Viscous Flows at Moderate and High Reynolds Numbers, Comput. Methods Eng. Sci. 16 (5) (2004) 441–451.
[25] J. Adams, P. Swarztrauber, R. Sweet, FISHPACK: A Package of Fortran Subprograms for the Solution of Separable Elliptic PDEs, The National Center for Atmospheric Research, Boulder, Colorado, 1980.
[26] R. Sweet, A cyclic reduction algorithm for solving block tridiagonal systems of arbitrary dimensions, SIAM J. Numer. Anal. 14 (1977) 706.
[27] A. Nicolás, B. Bermúdez, 2D thermal/isothermal incompressible viscous flows, Int. J. Numer. Methods Fluids 48 (2005) 349–366.
[28] J.P. Caltagirone, S. Bories, Solutions and stability criteria of natural convective flow in an inclined porous layer, J. Fluid Mech. 155 (1985) 267–287.
[29] R.A. Kuyper, Th.H. Van Der Meer, C.J. Hoogendoorn, R.A.W.M. Henkes, Numerical study of laminar and turbulent natural convection

in an inclined square cavity, Int. J. Heat Mass Transfer 36 (11) (1993) 2899–2911.

[30] N.C. Markatos, K.A. Pericleous, Laminar and turbulent natural convection in an enclosed cavity, Int. J. Heat Mass Transfer 27 (1984) 755–772.

[31] R.J.M. Bastiaans, C.C.M. Rindt, F.T.M. Nieuwstadt, A.A. van Steenhoven, Direct an large-eddy simulation of the transition of two and three-dimensional plane plumes in a confined enclosure, Int. J. Heat Mass Transfer 43 (2000) 2375–2393.

[32] F. Marcondes, J.M. De Medeiros, J.M. Gurgel, Numerical analysis of natural convection in cavities with variable porosity, Numer. Heat Transfer: Part A: Appl. 40 (4) (2001) 403–420.

[33] Hao D. Nguyen, Seungho Paik, Rod W. Douglass, Study of double-diffusive convection in layered anisotropic porous media, Numer. Heat Transfer: Part B: Fundam. 26 (4) (1999) 489–505.

[34] D.A.S. Rees, Darcy–Brinkman free convection from a heated horizontal surface, Numer. Heat Transfer: Part A: Appl. 35 (2) (1999) 191–204.